AIAA AVIATION Forum
June 25-29, 2018, Atlanta, Georgia
2018 AIAA/CEAS Aeroacoustics Conference

10.2514/6.2018-3606

Experimental investigation of the acoustic role of the output duct in the discharge of a high pressure flow through diaphragms and perforated plates.

Paul Laffay,*
Safran Aircraft Engines, 77500 Moissy-Cramayel, France and
Université de Lyon, École Centrale de Lyon, 69134 Écully, France
Marc C. Jacob ,†
ISAE-SupAéro, 31000 Toulouse, France and
Université de Lyon, École Centrale de Lyon, 69134 Écully, France
Stéphane Moreau‡
Université de Sherbrooke, Sherbrooke, J1K2R1 , Québec, Canada and
Université de Lyon, École Centrale de Lyon, 69134 Écully, France
Josselin Regnard,§
Safran Aircraft Engines, 77500 Moissy-Cramayel, France

This work presents the second step of an experimental study of the noise radiated by a complete flow discharge/control system allowing to expand or evacuate a flow under pressure by passing though diaphragms or perforated plates. The first step of the study, focused on the study of the noise radiated by the passage of the flow through the perforated plates/diaphragms, allowed to identify the presence of three distinct radiation sources: a broadband noise associated with the mixing of the flow at the exit of the perforations and which is strongly linked to the geometry, a shock noise (screech and broadband shock associated noise) associated with the presence of shock cells in the flow for supersonic regimes and a tonal noise associated with a feedback loop and appearing for low subsonic operating points. By adding a duct downstream to the discharge zone to be closer to real geometries found in industry, the broadband noise is strongly modify by the appearance of strong acoustic resonances in the outlet duct. These resonances are moreover strongly affected by the operating point which drives the flow intensity in the duct. A simple analytical model is proposed in order to quickly predict the different acoustic modifications induced by the outlet duct in case of simple geometries. Finally, the shock noise, as observed without duct, is totally suppressed but is replaced by "base-pressure oscillation" responsible for strong low frequency tones for diaphragms and perforated plates with large cross-sections.

I. Introduction

In a large number of industrial sectors, flow discharge or flow control systems can be found. In most cases, these systems are made by passing the flow through diaphragms or perforated plates. The passage of this flow through these pressure-reducing systems generates the appearance of high-speed jets often supersonic responsible for a very important acoustic radiation and even sometimes structural damages.
In an attempt to reduce the acoustic radiation of such devices, an experimental study has been carried out to

*PhD Student, Safran Aircraft Engines, Moissy-Cramayel and Université de Lyon, École Centrale de Lyon.
†Professor, ISAE-SupAro, Toulouse and Université de Lyon, École Centrale de Lyon, AIAA Member.
‡Professor, Université de Sherbrooke and Université de Lyon, École Centrale de Lyon, AIAA Lifetime Member.
§Acoustic Engineer, Safran Aircraft Engines, Moissy-Cramayel.

identify all the different acoustic sources responsible for this radiation and to propose solutions to attenuate or eliminate these sources. A first part of this study,[1] was focused on the acoustic radiation generated by the discharge of the high pressure flow through perforated plates and diaphragms. Indeed the passage of the flow through these perforations leads to very high speed jets responsible for an important acoustic radiation. As a reminder, the operating point in this study is defined by the ratio of the total pressure upstream of the grid or diaphragm p_t over the ambient pressure p_a and is called Nozzle Pressure Ratio (NPR). In this first step of the study, different acoustic behaviors have then been observed. For diaphragms, far field acoustic spectra is dominated by a mixing noise for all NPR and by a shock-associated noise (screech and broadband shock associated noise (BBSAN)) when the critical value of the NPR delimiting the subsonic and supersonic behavior (NPRc = 1.89) is exceeded. For perforated plates, the mixing noise is still present but is composed of two humps. The achieved parametric study allowed to associate the first hump to the noise of the downstream large equivalent jet formed from the mixing of all micro-jets while the second is associated with the noise of the outer micro-jets issuing from the perforations. The noise associated with supersonic phenomena (screech and BBSAN) has been observed for perforated plates only in the case of very close perforations. In this case, it behaves as a diaphragm.
In the present part of this study, the same simplified geometry is experimentally considered but with adding a pipe at the output of the sample holder (Fig. 1). This overall geometry is then closer to the geometry that can be found on real industrial systems.

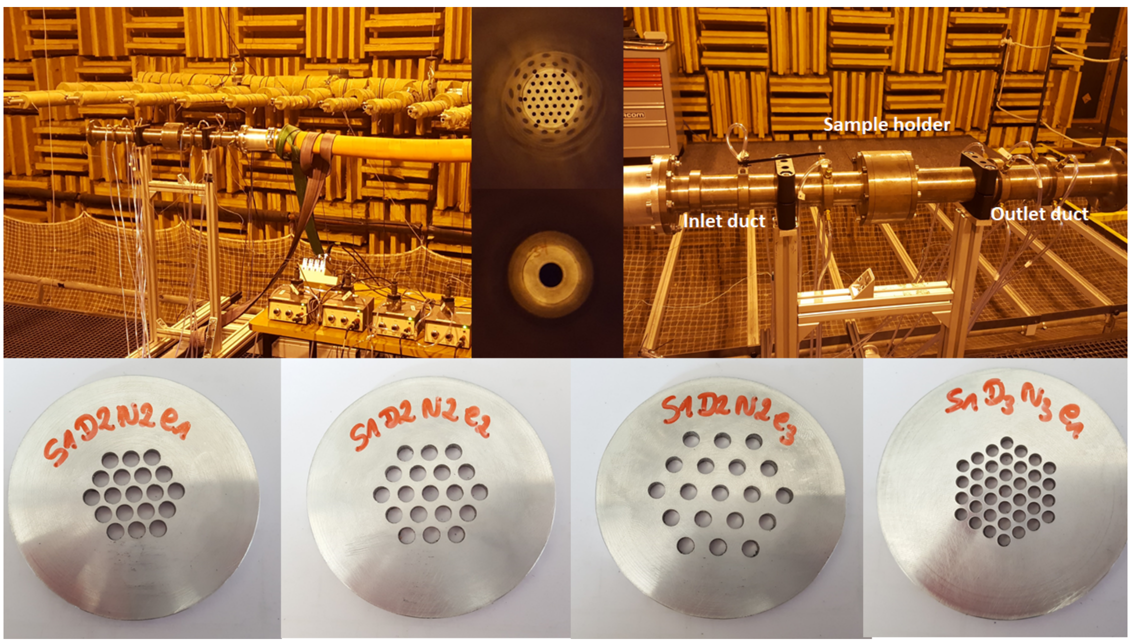

Figure 1. Experimental setup and a few samples tested

The objective of this part of the study is then to analyze the different acoustical effects of the outlet pipe on the noise generated.

II. Experimental set-up

The experiment has been carried out in the supersonic open-jet wind tunnel at École Centrale Lyon (ECL). The geometry studied is shown in Fig. 1. It consists of a cylindrical inlet duct of diameter D_e and length $6.1D_e$ leading to a sample holder that allows to insert different diaphragms or perforated plates that will generate a more or less important pressure drop. Downstream, an outlet duct of similar diameter and length $8.2D_e$ is added in order to be closer to the real industrial geometries. 3 diaphragms and 14 perforated plates (17 samples) have been tested. Characteristics of each sample are summarized in the table below. Samples are identified by the number of their perforations N, their diameter D, their mutual spacing e and their total area S. The different dimensions are normalized by D_e and S_e respectively the diameter and section of the outlet/inlet duct.

Name	N	D/D_e $\times10^{-1}$	e/D_e $\times10^{-1}$	S/S_e $\times10^{-2}$
S1	1	4.31	-	1.86
S1D1N1e1	7	1.63	0.20	1.86
S1D1N1e2	7	1.63	0.41	1.86
S1D1N1e3	7	1.63	0.82	1.86
S1D2N2e1	19	0.99	0.20	1.86
S1D2N2e2	19	0.99	0.41	1.86
S1D2N2e3/div/cong	19	0.99	0.82	1.86
S1D3N3e1	37	0.71	0.20	1.86
S1D3N3e2	37	0.71	0.41	1.86
S1D3N3e3	37	0.71	0.82	1.86
S2	1	2.61	-	0.68
S2D2N1e1	7	0.99	0.20	0.68
S3	1	6.01	-	3.61
S3D2N3e1	37	0.99	0.20	3.61
S4D4N4e4	351	0.31	0.06	3.29

Table 1. Geometric description of the diaphragms and perforated plates tested

For each sample, acoustic and aerodynamic measurements have been carried out from NPR= 1 to 3.6 by steps of 0.2. The acoustic measurements are performed with a far field directivity array placed at 2 m from the duct mouth and composed of 13 1/4 inch *Piezotronics PCB* microphones thus covering an observation angle Θ ranging from 30° to 150° by 10° steps. θ is defined with respect to the duct axis starting from downstream. Aerodynamic measurements consist of temperature, static and total pressure measurements. The total pressure measurement is achieved upstream of the sample holder in order to determine the operating point of the valve (NPR) while the static pressure measurements are made on both sides (ring of 4 pressure taps upstream and two rings of 4 pressure taps downstream). Finally, the temperature is measured at the inlet and outlet of the valve. More details can also be found in the first part of the study.[1]

III. Far field acoustic results without output duct

In the first part of the study without the outlet pipe, the major aeroacoustic behaviors caused by diaphragms or perforated plates have been identified. The ranges of presence of each of these phenomena are summarized in figure 2.

Three main different acoustic phenomena have then been identified: the mixing noise, the shock-associated noise and the low NPR tonal noise. The mixing noise, first of all, is a broadband radiation; it results from the mixing of the flow in the jet shear layers generated by the perforations and therefore appears for all the operation points and for all the configurations. In the case of the diaphragms, similar characteristics as the mixing noise of jet issuing from more conventional nozzles has been observed.[1] The shape of the far-field acoustic spectra agrees with Tam *et al.* similarity spectra[2] and the dual source of the mixing noise have been identified. In the case of the perforated plates, this mixing noise is strongly modified with the appearance of two distinct humps on the acoustic spectra. The high frequency hump has been attributed to the radiation of the small isolated jets issuing from the perforations while the low frequency one is attributed to the radiation of the merged jets that form an equivalent jet of larger diameter. The modification of the different geometrical parameters of the perforated plates will thus allow to adapt the radiation of the latter. For supersonic regimes, a shock-associated noise appears on diaphragms and on the perforated plates with very close perforations. This radiation is tonal (screech) and broadband (BBSAN) and is related to the interaction of instabilities in the shear layer with the shock cells present in the jet. The screech prediction models obtained on imperfectly expanded supersonic jets issuing from conventional convergent nozzles show

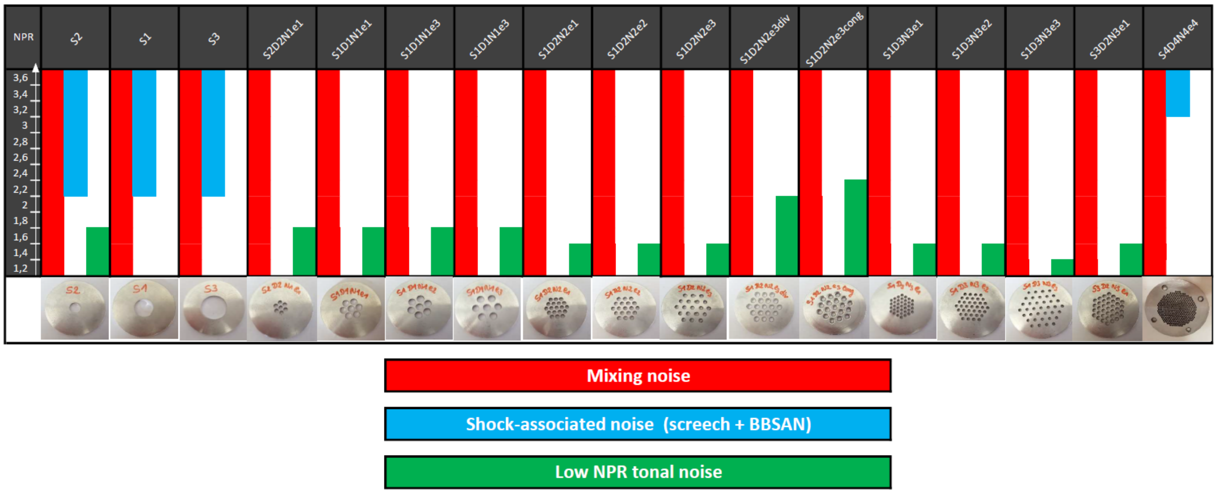

Figure 2. Summary of the present ranges of the different acoustic phenomena observed without the outlet duct

a good agreement with the results obtained on the diaphragm cases. Finally, a tonal radiation has also been observed for the low NPR on the majority of the perforated plates as well as on the smallest diaphragm. This radiation has been attributed to a feedback loop between instabilities in the flow due to sharp edges and abrupt section reduction and acoustic field .

IV. Far field acoustic results with output duct

In order to investigate the effects of the output duct, the far field acoustic spectra with and without output duct are now compared in Fig. 3 for the same configurations and for the microphone at 30°.

The different acoustic mechanisms present without the outlet duct are strongly altered and even sometimes suppressed.

First, for diaphragms, the shock-associated noise (screech denoted by the high frequency tones in Figs. 3 a) and c)) completely disappears. The broadband noise is also strongly modified with the outlet pipe: oscillations appear on the spectra probably due to the acoustic propagation in the duct. These oscillations will be studied in Sec. V. For the diaphragm S3, strong low frequency tones appear from NPR 2.2 to 3.4. Since the emergence of these tones appears at a particular NPR, there are probably not generated by the acoustic propagation in the duct as in the other configurations. In an attempt to validate this hypothesis, the bicoherence ($b(f_1, f_2)$) is plotted in Fig. 4 for configurations S1 and S3 at NPR 2.4. This signal processing tool allows finding the non linear interaction between two signals. it is expressed by the equation:

$$b(f_1, f_2) = \frac{|\sum_n F_n(f_1)F_n(f_2)F_n^*(f_1+f_2)|}{\sqrt{\sum_n |F_n(f_1)|^2|F_n(f_2)|^2|F_n^*(f_1+f_2)|^2}}, \tag{1}$$

where F denotes the Fourier transform and * the complex conjugate. Like the coherence, the bicoherence is bounded between 0 and 1. If it is equal to 1 between two frequencies f_1 and f_2, it means the frequency f_3=$f_1 + f_2$ is generated by a non linear interaction between the first two frequencies (in other words, the third frequency is not created by a new source).

Very different results are obtained between diaphragms S1 and S3 confirming the previous assumption. For S1, the bicoherence is equal to 0 for all frequencies. Therefore there is not any non-linear interaction, which is consistent with the assumption that oscillations in the spectra are due to the acoustic duct modes as discussed in Sec. V. However with the diaphragm S3, a bicoherence equal to 1 appears for each frequency of the high level peaks shown in Fig. 3 d. Thus, there is a strong non-linear interaction between the different tones, which suggest a new noise source. Moreover, for this regime, peaks also appear around 440 Hz, 880 Hz etc. which are also not consistent with the frequencies expected from the duct modes (see Sec. V). This radiation will be studied in more detail in Sec. VII. In fact, for the diaphragm S3, the oscillations associated

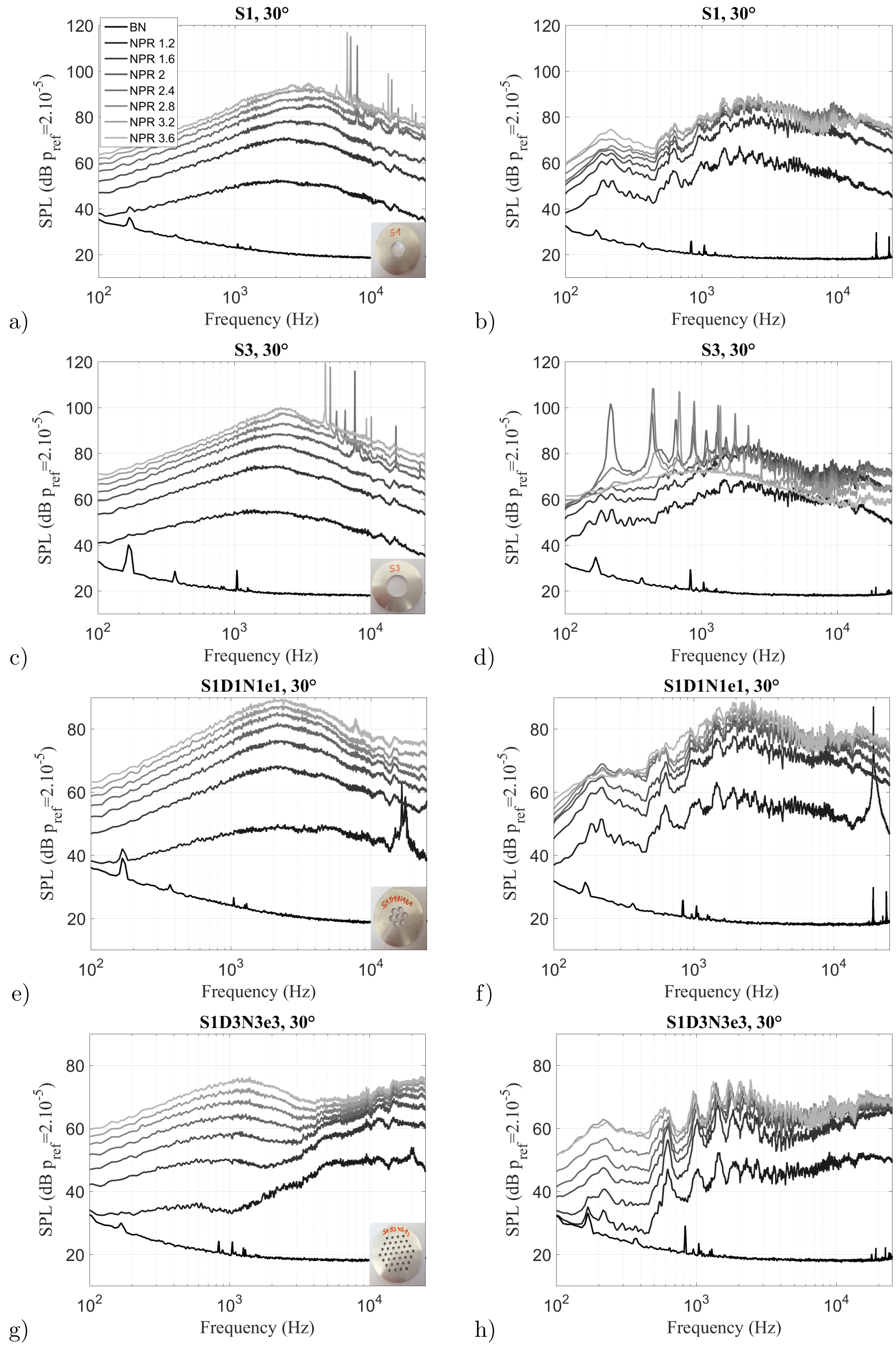

Figure 3. Comparison of the far field acoustic spectra for the configurations without output duct on the left and with output duct on the right for the perforated plates and diaphragms: a),b) S1, 30°**, c),d) S3,** 30°**, e),f) S1D1N1e1,** 30° **and g)h) S1D3N3e3,** 30°

with the propagation in the duct are less prononced than for smaller diaphragms (e.g. S1) especially at

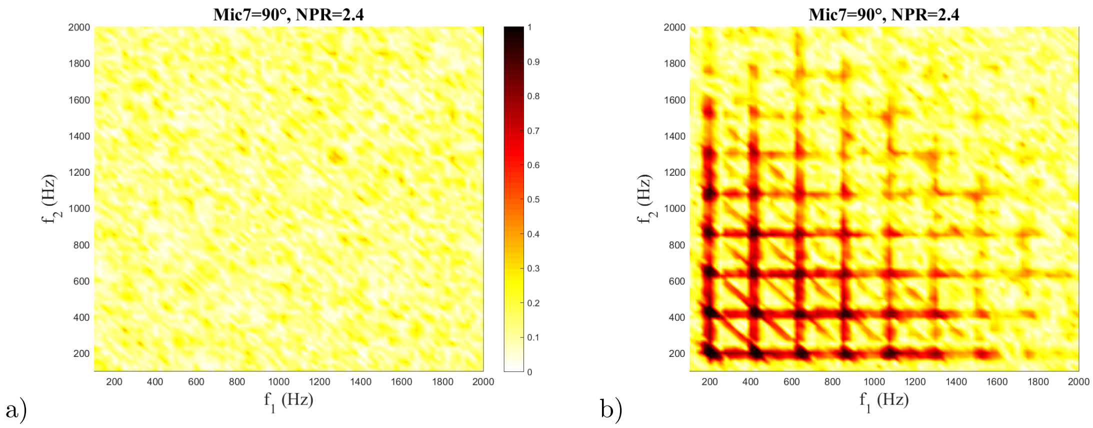

Figure 4. bicoherence for the configurations: a) S1, NPR 2.4**, b) S3, NPR** 2.4

higher frequencies (660 Hz...). This can be explained by the fact that with a larger diaphragm (S3), the flow rate is more important; thus the acoustic propagation is disturbed in the duct as discussed by Ingard and Singhal.[3]

For perforated plates (Fig. 3 c)-h)) the broadband noise is also strongly modified by the propagation in the duct. Oscillations seem to be more important when the perforation size decreases for a constant surface. The effect of the perforated plate/diaphragm geometry on these modal oscillations will be studied in Sec. V.

Moreover, even if the phenomenon is less pronounced, the two humps characteristic of the perforated plate mixing noise shown in Laffay *et al.*[1] are still present when the output duct is added. Indeed, for perforated plate with largely spaced perforations (Fig. 3 g) and h)), a significant increase of the high frequency noise appears. As discussed in Laffay *et al.*,[1] this phenomenon is caused by the radiation of the small isolated jets issuing from the perforations. Finally, the only acoustic behavior which seems to be not strongly modified by the output duct is the tonal noise at low NPR as shown in Figs. 3 e) and f). This radiation will be not analyzed in the present study.

To summarized, the different acoustic behaviors as well as the operating points of appearance of each regime are presented in Fig. 5.

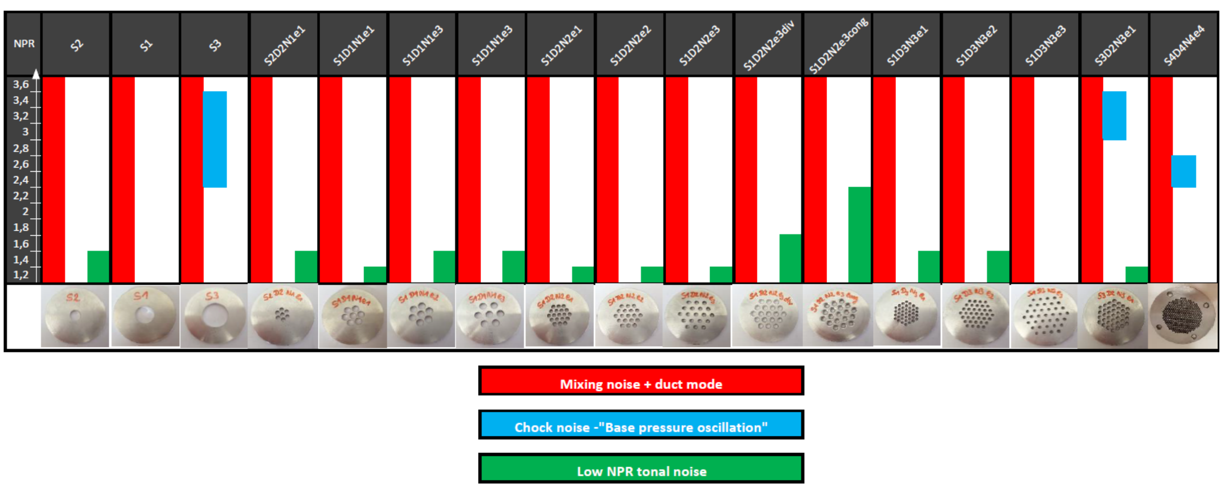

Figure 5. Summary of the present ranges of the different acoustic phenomena observed with the outlet duct

V. Study of propagation effects

In this part, a study of the sound propagation in the duct is conducted to highlight the different phenomena that are involved in the generation of the oscillations in the spectra. This problem has been extensively studied in aeroacoustics during the past years, for example in the context of sound radiation in turboengine ducts.[4] Indeed the propagation of the noise radiated by a source is strongly modified by the duct.

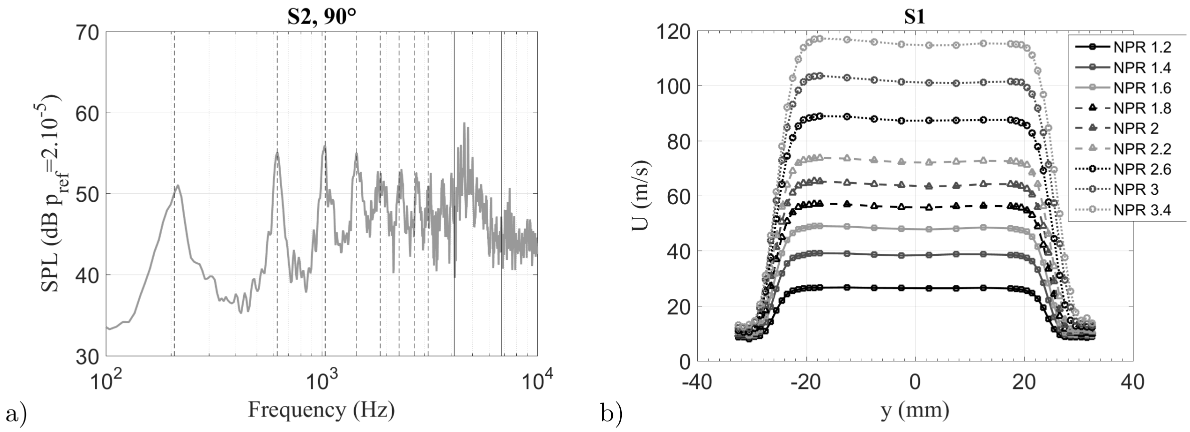

Figure 6. a)Far-field acoustic spectra for diaphragm S2 for $\theta = 90°$ and NPR$= 1.2$. b) Velocity profile at the exit of the outlet duct for diaphragm S1.

Two distinct mechanisms which may be responsible for the modification of the acoustic radiation with the duct have been identified. The first one is responsible for the slight jump of the spectra and the intensification of the oscillations seen for instance at 4200 Hz in Fig. 6. It is related to the way the sound is propagating in a duct. Indeed the acoustic pressure at any point of a duct can be expressed as an infinite sum of elementary wave patterns called modes. Depending on the frequency and the size of the duct, a mode can be cut-on or cut-off (except for the plane mode which is always cut-on). Thus for each mode there is a cut-off frequency f_c below which the mode does not propagate. By considering a 3D cylindrical duct of radius R, with hard wall and no mean flow, the acoustic pressure $p(x, r, \phi)$ at any point of the duct of axis x can be written with the following modal expression:[5,6]

$$p(x, r, \phi) = \sum_{m=-\infty}^{+\infty} \sum_{\mu=1}^{+\infty} \left(A_{m\mu} e^{-ik^+_{m\mu} x} + B_{m\mu} e^{-ik^-_{m\mu} x} \right) U_{m\mu}(r) e^{-im\phi}, \tag{2}$$

where $A_{m\mu}$ and $B_{m\mu}$ are the modal amplitudes and $k_0 = \frac{\omega}{c_0}$. $k^+_{m\mu}$ and $k^-_{m\mu}$ are the wave numbers of the two waves propagating in opposite directions and are given by:

$$k^+_{m\mu} = \sqrt{k_0^2 - \alpha^2_{m\mu}}, \qquad k^-_{m\mu} = -\sqrt{k_0^2 - \alpha^2_{m\mu}}. \tag{3}$$

From the boundary condition at $r = R$ (vanishing radial velocity), we have $\alpha_{m\mu} = \chi_{m\mu}/R$ with $\chi_{m\mu}$ the μ-th zero of the derivative of the Bessel function of the first kind J'_m *e.g.*:

$$J'_m(\alpha_{m\mu} R) = 0. \tag{4}$$

$U_{m\mu}(r)$ is the normalized mode and is defined by:

$$U_{m\mu}(r) = N_{m\mu} J_m(\alpha_{m\mu} r), \tag{5}$$

where $N_{m\mu}$ is the normalization coefficient calculated from $\int_0^R N^2_{m\mu} J_m(\alpha_{m\mu} r)^2 r dr = 1$ and is equal to:

$$N_{m\mu} = \frac{\sqrt{2}}{J_m(\alpha_{m\mu} R) \sqrt{R^2 - \frac{m^2}{\alpha^2_{m\mu}}}} \tag{6}$$

for each mode except for the plane mode where $N_{01} = \frac{\sqrt{2}}{R}$. Finally, a wave can propagate in the duct if $k_0^2 - \alpha_{mn}^2 > 0$ (Eq. 3). The cut-off frequency is then given by:

$$k_0^2 - \frac{\chi_{mn}^2}{R^2} > 0 \quad \Rightarrow \quad f_c = \frac{\chi_{mn} c_0}{2\pi R}. \tag{7}$$

The first two passing modes (fist two azimutal modes) are the modes $(1,1)$ and $(2,1)$ respectively ,and $\chi_{1,1} = 1.84$, $\chi_{2,1} = 3.05$. The cut-off frequency in each case is then $f_{c_{1,1}} = 4124$ Hz and $f_{c_{2,1}} = 6835$ Hz for the present duct dimensions. These frequencies are represented by the black lines in Fig. 6 and coincides with the slight jumps in the spectra quite well. In the present case the best prediction is obtained by considering a zero mean flow in the output duct. To recall, the cut-off frequency with mean flow is:

$$f_c = \frac{\chi_{mn} c_0}{2\pi R}\sqrt{1 - M_x^2} \tag{8}$$

with M_x the mean Mach number of the flow in the outlet duct.
The second mechanism that can yield the oscillations is linked to longitudinal resonances in the ouptut pipe as in a musical instrument. Indeed the acoustic wave that is generated at the output of the perforated plates or diaphragms propagates in the duct to the outlet. Part of the wave will therefore come out of the duct and radiate outside but another part is reflected and goes in the opposite direction.[7] Part of the latter wave is then reflected on the sample and so on creating resonances in the duct for some characteristic frequencies depending on the length of the outlet pipe. An estimate of the longitudinal resonance frequency $f_{r,n}$ can be easily calculated by considering a plane wave in a 1D open-ended tube of length L with no mean flow. The acoustic pressure $p(x)$ is then:

$$p(x) = Ae^{ik_0 x} + Be^{-ik_0 x}. \tag{9}$$

The boundary conditions are moreover: $u(x = 0) = 0$ and $p(x = L) = 0$. The linearized Euler equations first give:

$$\frac{\partial p}{\partial x}(x = 0) = 0 \quad \Rightarrow \quad A = B \tag{10}$$

and the boundary condition at $x = L$ reads:

$$2A\cos(k_0 L) = 0. \tag{11}$$

This condition is finally validated if:

$$f_{r,n} = (2n - 1)\frac{c_0}{4L}, \tag{12}$$

with n a positive integer. This relation thus gives the resonance frequencies of a 1D open ended duct of length L with no mean flow. However, Numerous studies have shown that this relationship does not predict perfectly the frequencies observed in the case of real ducts. Indeed, for real geometries, it is necessary to take into account a correction of the length δ due to the finite cross-section of the duct which generates a slight deformation of the plane mode becoming slightly spherical. The reflection of the wave is then no longer perfectly at the exit of the duct but slightly further. For an unflanged duct with no mean flow, the correction is $\delta \simeq 0.61R$.[3,6,7] By considering the corrected length of the present output duct $L' = L + \delta$, the first resonance frequencies are summarized in the Tab. 2 and are represented by the black dash lines in Fig. 6. These resonant frequencies coincide very well with the strong oscillations present in the spectra.

n	1	2	3	4	5	6	7	8
$f_{r,n}$ (Hz)	207.8	623.4	1039.1	1454.7	1870.4	2286.0	2701.6	3117.3

Table 2. Resonant frequencies for the present geometry without flow.

In the same way as previously, for the present case (small diaphragm and low NPR), the best prediction is obtained by considering a zero mean flow in the output duct. For configurations with larger diaphragm/perforated plate as well as NPR, taking into account a mean flow in the outlet duct may improve the prediction. To recall, the resonance frequency with flow is given by:

$$f_{r,n} = (2n - 1)(1 - M_x^2)\frac{c_0}{4(L + \delta)}. \tag{13}$$

In the case of a low mean flow Ingard and Singhal[3] propose a duct length correction equal to: $\delta \simeq 0.61R(1-M_x^2)$
The interest is now focused on the effect of the operating point and therefore of the flow velocity at the outlet duct on the resonance intensities and frequencies. For this purpose, the difference of sound pressure level between the configuration with the outlet duct and without the outlet duct is shown in the maps in Fig. 7. This acoustic pressure difference allows to highlight only the acoustic effects related to the presence of the output duct and is calculated from:

$$\Delta SPL = 10 \log \left(\frac{Spp_{WD}}{Spp_{WOD}} \right), \tag{14}$$

where Spp_{WD} and Spp_{WOD} are respectively the power spectral density of the acoustic signal for the configuration with duct and without duct. For the three presented cases, it can be seen that the longitudinal resonance frequencies do not vary significantly as a function of the NPR and therefore of the flow velocity in the generated jet and in the outlet duct. The frequency of the standing wave seems thus to be not significantly affected by the convection of the flow velocity in the outlet duct. By considering the previous relationship and a mean flow of $U = 100$ m/s which corresponds approximately to the speed of the flow at the exit of the outlet duct for the perforated plates and diaphragm with section S1 and NPR= 3 (Fig. 6 (b)), the predicted frequency offset taking into account the flow is only of 8.1% compared with the prediction without flow and drops to 0.5% for a mean flow of 25 m/s typical of a NPR= 1.2 for S1. The frequency shift therefore remaining quite low, especially for the lowest regimes where the resonances are the most marked, we can assume that this shift is masked by the peak width induced by the resonances as well as by the use of the logarithmic scale on the plots. A strong decrease in the amplitude of these resonances can also be observed when the NPR and therefore the speed of the flow increases. This observation is consistent with the work of Ingard and Singhal[3] and they explain this attenuation by the interaction of the sound field with the turbulent flow in the duct as well as by the modification of the output impedance of the duct. It also seems by comparing the two perforated plates with similar cross-section in Figs. 7 b) and c) that the geometry of the perforated plates has a significant influence on this attenuation. Indeed, we can suppose that the more or less late mixing of the micro-jets, induced by the size and the spacing of the perforations, will generate a significant modification of the turbulence scales and mixing, leading therefore to a modification of the interaction with the acoustic field and a modification of the attenuation.

A similar analysis is achieved for a constant NPR but by varying the observation angle Θ (Fig. 8). As espected, no change in the resonance frequencies as a function of the observation angle is observed for a given NPR. However, a variation of the intensity of these resonances can be observed. In particular for $\Theta = 30°$, there is a strong decrease of the amplitude resonances. This can perhaps be explained by the stronger emergence of the output jet noise in this direction.[1,2] For $\Theta > 90°$, a strong attenuation of the resonances beyond 2000 Hz also appears. This attenuation is found in a majority of the studied configurations and may be explained by some acoustical reflections on the outlet surface of the duct.

VI. Analytical modeling of the output duct

In an attempt to predict the acoustic modification induced by this kind of simple duct geometry, it is possible to propose a simple analytical model of the outlet pipe. The duct is modelled as a 3D cylindrical pipe of radius R and length L with rigid walls and without flow. One end of the duct is considered closed and the other open. At the closed end of the duct, a modal source is added to simulate the radiation of the perforated plates and diaphragms. At the open end, an output impedance is used in order to account for the acoustical reflection and radiation by the aperture. This impedance is derived from the work of Zorumski[8] as well as Shao and Mechefske.[9] This impedance is calculated from a Helmholtz integral which allows linking the pressure outside of the duct to the axial velocity in the output section in the case of a cylindrical duct with infinite flange. In other words, this output section acts as a piston.
As given in the previous section, the pressure in the duct is expressed as:

$$p(x, r, \phi) = \sum_{m=-\infty}^{+\infty} \sum_{\mu=1}^{+\infty} P_{m\mu} U_{m\mu}(r) e^{-im\phi}, \tag{15}$$

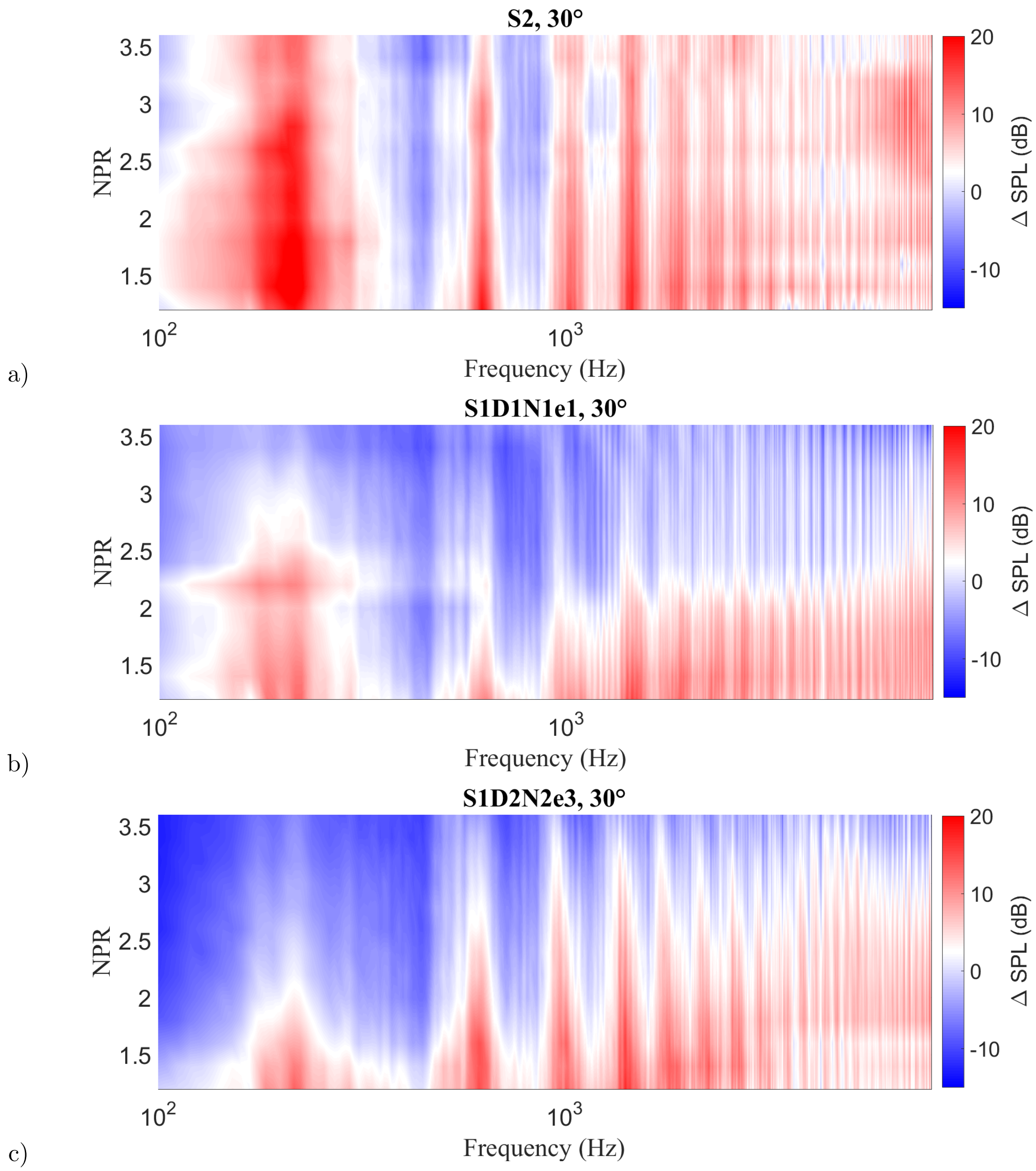

Figure 7. Map of ΔSPL as a function of the NPR for: a) S2, b)S1D1N1e1 and c)S1D2N2e3.

where: $P_{m\mu} = A_{m\mu}e^{-ik^{+}_{m\mu}x} + B_{m\mu}e^{-ik^{-}_{m\mu}x}$, $U_{m\mu}(r) = N_{m\mu}J_m(\alpha_{m\mu}r)$, $\alpha_{m\mu} = \chi_{m\mu}/R$ and $k_0^2 = \alpha_{m\mu}^2 + k_{m\mu}^2$. For future mathematical convenience, the modal normalization is calculated this time by considering:

$$k_0^2 \int_0^R N_{m\mu}^2 J_m(\alpha_{m\mu}r)^2 r dr = 1, \tag{16}$$

which gives: $N_{m\mu} = \frac{1}{k_0 R\left[\frac{1}{2}\left(\frac{\alpha_{m\mu}^2R^2-m^2}{\alpha_{m\mu}^2R^2}\right)J_m(\alpha_{m\mu}R)^2\right]^{1/2}}$. Linearized Euler equations along the x axis allow to express velocity in this direction:

$$\rho\frac{\partial U_x}{\partial t} = -\frac{\partial p}{\partial x}, \tag{17}$$

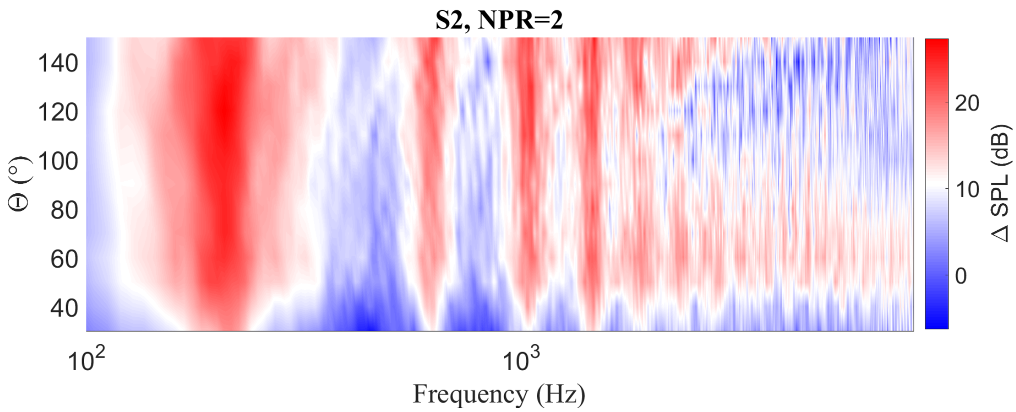

Figure 8. Map of ΔSPL as a function of the observation angle Θ for: a) S2 at NPR$=2$.

which gives:

$$u_x(x,r,\phi) = \frac{1}{\rho c_0} \sum_{m=-\infty}^{+\infty} \sum_{\mu=1}^{+\infty} V_{m\mu} U_{m\mu}(r) e^{-im\phi}, \tag{18}$$

with $V_{m\mu} = -A_{m\mu}\frac{k^+_{m\mu}}{k_0}e^{-ik^+_{m\mu}x} - B_{m\mu}\frac{k^-_{m\mu}}{k_0}e^{-ik^-_{m\mu}x}$. At $x=0$, an acoustic source simulating the radiation of the diaphragms and perforated plates is added. This source excites each mode of the same amplitude S_0 and is therefore expressed by:

$$S = S_0 \sum_{m=-\infty}^{+\infty} \sum_{\mu=1}^{+\infty} N_{m\mu} J_m(\alpha_{m\mu} r) e^{-im\phi}. \tag{19}$$

At $x=0$, the total reflection of the pressure implies: $P^+ = S + P^-$ *e.g.*:

$$\sum_{m=-\infty}^{+\infty} \sum_{\mu=1}^{+\infty} U_{m\mu}(r) A_{m\mu} e^{-im\phi} = S0 \sum_{m=-\infty}^{+\infty} \sum_{\mu=1}^{+\infty} U_{m\mu}(r) e^{-im\phi} + \sum_{m=-\infty}^{+\infty} \sum_{\mu=1}^{+\infty} U_{m\mu}(r) B_{m\mu} e^{-2ik^+_{m\mu}L} e^{-im\phi}. \tag{20}$$

The term $e^{-2ik^+_{m\mu}L}$ expresses the phase shift of the reflected wave with respect to the incident wave. In particular, one solution of this equation is:

$$A_{m\mu} = S_0 + B_{m\mu} e^{-2ik^+_{m\mu}L}. \tag{21}$$

At $x=L$, Zorumski's output duct impedance is imposed; it is expressed as:

$$P_{m\mu}(L) = \sum_{l=1}^{+\infty} Z_{m\mu l} V_{ml}(L), \tag{22}$$

with:

$$Z_{m\mu l} = \int_0^{\pi/2} \sin(\Phi) D_{m\mu}(\sin(\Phi)) D_{ml}(\sin(\Phi)) d\Phi - i \int_1^{\infty} \cosh(\xi) D_{m\mu}(\sin(\xi)) D_{ml}(\sin(\xi)) d\xi \tag{23}$$

and

$$D_{m\mu}(\tau) = \frac{k_0^2 R}{(\tau k_0)^2 - (\alpha_{m\mu})^2} \left[\tau k_0 J'_m(\tau k_0 R) J_m(\alpha_{m\mu} R)\right]. \tag{24}$$

Eq. (22) gives:

$$A_{m\mu} e^{-ik^+_{m\mu}L} + B_{m\mu} e^{-ik^-_{m\mu}L} = \sum_{l=1}^{+\infty} Z_{m\mu l} \left[-A_{ml}\frac{k^+_{ml}}{k_0} e^{-ik^+_{ml}L} - B_{ml}\frac{k^-_{ml}}{k_0} e^{-ik^-_{ml}L}\right]. \tag{25}$$

By relating the coefficients A and B thanks to Eq. (21), we finally have:

$$\sum_{l=1}^{+\infty} S_0 \left[Z_{m\mu l} \frac{k_{ml}^{+}}{k_0} e^{-ik_{ml}^{+}L} + \delta_{\mu l} e^{-ik_{m\mu}^{+}L} \right] = \sum_{l=1}^{+\infty} B_{ml} \left[-Z_{m\mu l} \frac{k_{ml}^{+}}{k_0} e^{-2ik_{ml}^{+}L} - \delta_{\mu l} e^{-2ik_{m\mu}^{+}L} \right] \tag{26}$$

This system of equation can be solved by truncating the number of modes in the infinite sums, which allow to obtain the coefficients $B_{m\mu}$. Having now the expression of the acoustic pressure and velocity in the duct, it is possible to express the acoustic transmission loss TL generated by this one. It is expressed by the ratio of the acoustic power at the exit of the duct Π_o over the acoustic power generated by the source Π_s:

$$TL = 10 \log \left(\frac{\Pi_o}{\Pi_s} \right), \text{ with } \Pi = \int_0^{2\pi} \int_0^{R} \frac{1}{2} Re\left(p(x,r,\phi) u_x^{*}(x,r,\phi) \right) r dr d\phi. \tag{27}$$

In order to simplify the expression of the power, the azimuthal modes are considered independent, which means that a given azimutal mode m will be unchanged throughout the duct. Moreover, the different modes forming an orthogonal base, the preceding expression can be simplified by:

$$\Pi = \frac{c_0}{2\rho f} Re \left(\sum_{m=-\infty}^{+\infty} \sum_{\mu=1}^{+\infty} P_{m\mu}(x) V_{m\mu}^{*}(x) \right). \tag{28}$$

Based on this model, the calculated TL is compared with the far-field acoustic spectra in the case of the diaphragm S2 and NPR= 1.2 in Fig. 9. For this experimental configuration, the operating point is low and the diaphragm is small so that the experimental conditions are close to the assumptions made for the model (no flow in the outlet duct). Despite slightly different levels, it can be seen that this simple modeling makes it possible to predict the main acoustic changes generated by the output duct. Indeed, on the TL curve the different oscillations induced by the longitudinal resonances of the duct can be seen as well as the appearance of the first azimutlal mode at 4124 Hz highlighted by the oscillation densification and the brutal level jump. A slight frequency shift of the different modes can also be observed especially for the higher frequencies and is probably explained by the absence of flow in the model.
Thus, the combination of this kind of simple modeling with jet or grid noise models as given in Tam *et al.*[2] and Laffay *et al.*[1] will allow rapidly predicting the broadband radiation generated by this type of discharge systems in the case of a fairly simple duct geometry. Indeed, the curve ΔSPL in Fig. 9 show that in cases where only jet mixing noise occurs (no tonal regimes), it seems that the main effect of the addition of the output duct is the appearance of these different acoustic modes/resonances that can be quite easily predicted. For more complex geometries, it will be thus probably interesting to separate the study in two steps: to study on one side the radiation associated with the jet mixing noise (the source) by using simple models or by simulation (complex) and on the other side to study acoustic propagation effects related to the actual geometry of the duct by simulation.

VII. Study of the shock noise

The bicoherence study showed that the tonal noise that appeared for $2.4 \leq NPR \leq 3.4$ for diaphragm S3 as well as perforated plates S3D2N3e1 ($3 \leq NPR \leq 3.4$) and S4D4N4e ($2.4 \leq NPR \leq 2.6$) is not generated by the same phenomena (acoustic resonances) like in others configurations.
Several studies have been conducted in the past both numerically and experimentally on the aeroacoustic phenomena that appear when a transsonic flow passes through a sudden duct expansion.[10–14] Depending on the NPR, they have shown the emergence of different behaviors that may be responsible for a significant acoustic radiation. Similar phenomenon can occur in the present case. In the case of a duct with a rectangular cross-section, Anderson *et al.*[13] observed for the highest NPR, the appearance of a series of oblique shock cells along the entire length of the output duct following the sudden expansion. This is a stable behavior. By now reducing the NPR, this oblique shock pattern is decreased in length and the end of the chock cells comes closer to the section expansion. The behavior then becomes unstable due to the distortion of the shock-wave pattern and cause the appearance of random pressure oscillations at the outlet of the duct. By further reducing the NPR, a new unsteady regime appears in the transition from oblique shocks pattern to a single normal shock. Indeed during a complete period of this regime, the shock structure goes from an oblique pattern to a normal one. When the NPR is reduced again, the regime becomes stable with a single

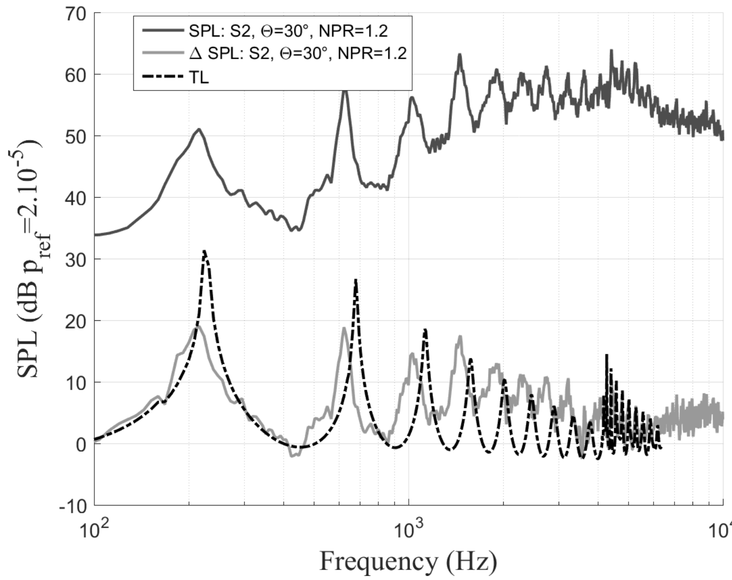

Figure 9. Comparison of the experimental acoustic spectra for S2 at NPR$= 1.2$ with the transmission loss TL calculated.

normal shock at the exit of the expansion. This shock reaches the walls of the outlet duct so that, in the same way as for the previous cases, the flow upstream is totally supersonic and no disturbance can travel until the upstream corners. However, once again reducing the pressure ratio, the intensity of the normal shock decreases and no longer reaches the walls of the duct. As a result, the flow becomes subsonic in the boundary layers and upstream of the shock between the core flow boundaries and the walls, allowing the travel of disturbances upstream. Strong pressure oscillations can thus appear at the corners of the expansion that are no longer dead zones and generates an unstable regime called "base pressure oscillations". This regime can also appear in the case of a cylindrical duct.[12,13] The self-exciting mechanism of this last behavior is irregular but can sometimes be locked on the longitudinal resonance frequencies of the outlet duct creating a strong coupling and generating a very important acoustic radiation and can explain the strong tones that appear on the diaphragm S3 and perforated plates S3D2N3e1 and S4D4N4a4 at high NPR.

As proposed by Emmert *et al.*,[14] the fundamental frequency of this coupling can thus be approximated by considering an 1D open-ended tube of length L. This regime appearing on the diaphragms, and perforated plates with a large cross-section ($S/S_e > 3.29 \times 10^{-2}$) and for high NPR, it may be interesting to take into account here a flow in the outlet duct. The longitudinal resonance frequencies $f_{r,n}$ are then given by the previous Eq. (13) with M_x the mean Mach number behind the normal shock. By considering a perfectly expanded jet, the mean Mach number of the jet issuing from the diaphragm/perforated plate can be approximated from the NPR by using the following isentropic relationship:

$$M_j = \sqrt{\frac{2}{\gamma - 1}\left[NPR^{\frac{\gamma-1}{\gamma}} - 1\right]}, \tag{29}$$

where γ is the air heat capacity ratio. From, the total temperature T_t measured in the jet in the configuration without output duct, it is possible to calculate the static temperature T_s of this jet with:

$$T_j = \frac{T_t}{1 + M_j^2(\gamma - 1)/2}. \tag{30}$$

The velocity of the perfectly expanded flow is finally:

$$U_j = M_j\sqrt{\gamma r T_j}. \tag{31}$$

By considering the conservation of mass-flow rate, the mean velocity in the output duct U_x is then:

$$U_x = \frac{\rho_j U_j S}{\rho_e S_e}, \tag{32}$$

with S_e the section of the output duct and ρ_j and ρ_e the density of the flow in the jet and in the output duct respectively. Supposing $\rho_j = \rho_e$, the Mach number in the output duct is then:

$$M_x = \frac{U_j S}{S_e c_e}, \tag{33}$$

with c_e the speed of sound in the output duct assumed equal to the ambient one. The fundamental frequency of the base pressure oscillation given by the first longitudinal resonance frequency of the duct can thus be calculated and is summarized in Tab. 3. For any flow condition, the first longitudinal frequency of the duct is $f_{r,1} = 207.8$ Hz. These fundamental frequencies are given in Fig. 10 by the straight lines in black by considering a mean flow and in red without flow respectively. The doted lines gives the harmonics of these fundamental frequencies.

	S3/S3D2N3e1						S4D4N4e4	
NPR	2.4	2.6	2.8	3.0	3.2	3.4	2.4	2.6
M_j	1.19	1.25	1.31	1.36	1.40	1.45	1.19	1.25
M_e	0.39	0.40	0.41	0.43	0.44	0.45	0.35	0.37
$f_{r,1}$ (Hz)	178	175	173	171	169	168	183	181

Table 3. Fundamental frequencies of the base pressure oscillation.

First of all, significant differences between predictions and measurements are seen in all cases. For the configuration S3 and S3D2N3e1, the best prediction is given by the model without flow while for S4D4N4e4, the model with flow gives better results. The grid S4D4N4e4 having perforations on the whole section of the duct (diameter of the circumscribed circle to the perforations equal to the diameter of the output duct), we can suppose that the boundary layer thickness is then decrease and the speed of the flow in close to the duct wall is then not negligible unlike the two other cases. An analysis of the flow would nevertheless be necessary to validate this hypothesis. For the configurations S3 with $2.8 \leq NPR \leq 3.4$, the base pressure oscillation frequency seems still based on the first longitudinal resonance although this fundamental frequency does not appear in acoustic spectra. In these cases, only one harmonic out of two (NPR= 2.8 and 3) or three (NPR= 3.2 and 3.4) radiates. No explanation has yet been reached to explain this phenomenon.

VIII. Conclusion

An experimental study of the noise generated by a complete flow discharge system (perforated plate or diaphragm associated with a output duct) has been conducted. By considering only the discharge of the high pressure flow though diaphragm or perforated plates without duct, three distinct radiation sources can be identified:[1] a broadband noise induced by the mixing of the jets issuing from the perforations, a tonal noise appearing for supersonic operating points and generated by the appearance of a feedback loop between shock cells and instability wave and a tonal noise appearing for low subsonic operating points and resulting for a feedback loop between acoustic field and flow in the perforations.

Yet, adding a duct downstream to these perforated plates/diaphragms yields significant changes of the acoustic radiation. First, the broadband noise is strongly modified with the appearance of strong resonances linked to the geometry of the outlet duct and in particular, the length, which sets the standing wave frequencies. These resonances have moreover shown to be strongly affected by the flow in the output duct. Indeed, the increase of the operating point and thus of the flow speed in the outlet duct generates a significant reduction of the resonance amplitudes, probably due to the interaction of the turbulence with the acoustic field as well as to the convective effects (synchronization of opposite direction waves). The resonance frequencies, however, showed to not be significantly affected by the increase of the operating point. A simple analytical model has also been proposed in order to predict the different acoustic modifications induced by the outlet duct. For supersonic regimes, the shock noise (screech and broadband shock associated noise)

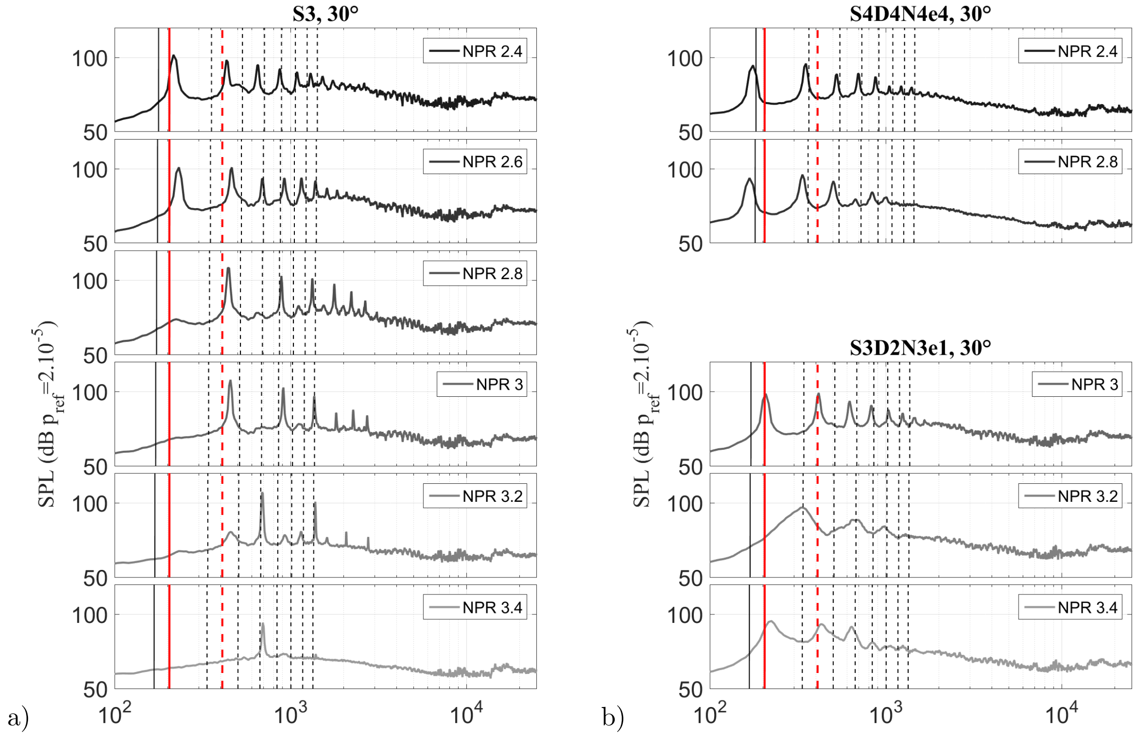

Figure 10. Summary of the present ranges of the different acoustic phenomena observed with the outlet duct

observed in the case without output duct totally disappear but is replaced by "base pressure oscillations" for diaphragms and perforated plates with large cross section. This acoustic behavior induces high low frequency tones and result for the oscillation of the normal shock appearing at the outlet of the perforated plates. As observed in previous works,[14] this oscillation seems to be locked on the first longitudinal resonance of the output duct.

Acknowledgements

This work was performed within the framework of the Labex CeLyA of the Université de Lyon, within the programme "Investissements d'Avenir" (ANR-10- LABX-0060/ANR-11-IDEX-0007) operated by the French National Research Agency (ANR) and is also supported by the industrial Chair ADOPSYS co-financed by Safran Aircraft Engines and the ANR (ANR-13-CHIN-0001-01).

References

[1]Laffay, P., Jacob, M., Moreau, S., and Reignard, J., "Experimental investigation of transient bleed vavlve noise," *23nd AIAA/CEAS Aeroacoustics Conference*, Denver, CO, USA, 2017.

[2]Tam, C., Golebiowski, M., and Seiner, J., "On the two Components of Turbulent Mixing Noise from Supersonic Jets," *2nd AIAA/CEAS Aeroacoustics Conference*, State Collage, PA, USA, 1996.

[3]Ingard, U. and Singhal, V., "Effect of flow on the acoustic resonances of an open-ended duct," *Journal of the Acoustical Society of America*, Vol. 58, No. 4, 1975, pp. 788–793.

[4]Druon, Y., "Étude de la propagation guidée et rayonnment acoustiques par les conduits d'jection de turboracteur," *PhD Thesis, École Centrale Lyon*, 2006.

[5]Rienstra, S. and Hirshberg, A., "An introduction to acoustics," *Technische Universiteit Eindhoven*, 2004.

[6]Rienstra, S. and Hirshberg, A., "Fundamentals of duct acoustics," *Technische Universiteit Eindhoven*, 2015.

[7]Levine, H. and Schwinger, J., "On teh radiation of sound from an unflanged circular pipe," *Physical review*, Vol. 73, No. 4, 1948, pp. 383–406.

[8]Zorumski, W., "Generalized radiation impedances and reflction coefficients of circular and annular ducts," *Journal of the Acoustical Society of America*, Vol. 54, No. 6, 1973, pp. 1667–1673.

[9]Shao, W. and Mechefske, C., "Analyses of radiation impedances of finite cylindrical ducts," *Journal of Sound and Vibration*, Vol. 286, 2005, pp. 363–381.

[10]Meier, G., Grabitz, G., Jungowski, W., Witczak, K., and Anderson, J., "Oscillations of the supersonic flow downstream of an abrupt increase in duct cross section," *AIAA Journal*, Vol. 18, No. 4, 1980, pp. 394–395.

[11]Meier, G., Szumowski, P., and Selerowicz, W., "Self-excited oscillations in internal transonic flows," *Prog. Aerospace Sci.*, Vol. 27, 1990, pp. 145–200.

[12]Anderson, J. and Williams, T. J., "Base pressure and noise produced by the abrupt expansion of air in a cylindrical duct," *J. Mechanical Engineering Science*, Vol. 10, No. 3, 1968, pp. 262–268.

[13]Anderson, J., Jungowski, W., Hiller, W., and Meier, G., "Flow oscillation in a duct with a rectangular cross-section," *J. Fluid Mech.*, Vol. 79, No. 4, 1977, pp. 769–784.

[14]Emmert, T., Lafon, P., and Bailly, C., "Numerical study of self-induced transonic flow oscillations behind a sudden duct enlargement," *Physics of fluids*, Vol. 21, 2009.